Electronic Supplementary Information

Catalytic water oxidation by an *in-situ* generated ruthenium nitrosyl complex bearing a bipyridine-bis(alkoxide) ligand

Yingying Liu,*[a] Siu-Mui Ng,[b] Shek-Man Yiu[c] and Tai-Chu Lau *[c]

[a] Institute of Intelligent Machines, Hefei Institutes of Physical Science,

Chinese Academy of Sciences, Hefei 230031, P. R. China.

Email: yyliu@iim.ac.cn

[b] Department of Food and Health Sciences,

Technological and Higher Education Institute of Hong Kong (THEi),

20A Tsing Yi Road, Tsing Yi Island, Hong Kong SAR, P. R. China.

[c] Department of Chemistry,

City University of Hong Kong, Tat Chee Avenue, Kowloon Tong, Hong Kong SAR, P. R. China.

E-mail: bhtclau@cityu.edu.hk

Index *Page*

Table S1 Selected bond lengths (Å) and angles (°) for **2**[$Ce(NO_3)_6$] and **3**[PF_6]$_2$.

2[$Ce(NO_3)_6$]				**3**[PF_6]$_2$			
Ru1–O1	1.8983	O1–Ru1–N4	96.825	Ru1–O3	2.0096	N1–Ru1–N4	92.321
Ru1–O2	1.9049	O1–Ru1–N2	148.663	Ru1–N1	1.7635	N1–Ru1–N5	90.757
Ru1–N1	2.0160	O1–Ru1–N3	80.846	Ru1–N2	2.2049	N2–Ru1–O3	157.867
Ru1–N2	2.0120	O2–Ru1–N1	149.411	Ru1–N3	2.0096	N2–Ru1–N3	78.066
Ru1–N3	2.1018	O2–Ru1–N2	77.806	Ru1–N4	2.1003	N2–Ru1–N4	91.359
Ru1–N4	2.0972	O2–Ru1–N3	97.178	Ru1–N5	2.1080	N2–Ru1–N5	91.572
		O2–Ru1–N4	80.530	O1–N1	1.1419	N3–Ru1–O3	79.866
		N1–Ru1–N2	76.481	O2–H2	0.8402	N3–Ru1–N4	88.565
		N1–Ru1–N3	96.925			N3–Ru1–N5	87.835
		N1–Ru1–N4	87.473			N4–Ru1–O3	86.394
		N2–Ru1–N3	85.252	N1–Ru1–O3	92.659	N4–Ru1–N5	174.796
O1–Ru1–O2	131.615	N2–Ru1–N4	99.164	N1–Ru1–N2	109.441	N5–Ru1–O3	89.274
O1–Ru1–N1	77.499	N3–Ru1–N4	174.417	N1–Ru1–N3	172.407	Ru1–N1–O1	171.653

Table S2. Crystal data and structure refinement details for **2**[$Ce(NO_3)_6$] and **3**$[PF_6]_2$.

	2[$Ce(NO_3)_6$]·$3CH_3CN$ (CCDC No.: 2084830)	**3**$[PF_6]_2$·$2H_2O$ (CCDC No.: 2084831)
Empirical formula	$C_{34}H_{41}CeN_{13}O_{20}Ru$	$C_{28}H_{37}F_{12}N_5O_5P_2Ru$
Formula weight	1192.99	914.63
Crystal system	triclinic	triclinic
Space group	P -1	P -1
a/Å	11.4188(4)	10.5197(4)
b/Å	12.6730(4)	11.3197(5)
c/Å	16.9821(5)	15.7798(6)
α/deg	88.005(2)	86.519(3)
β/deg	89.737(3)	80.554(3)
γ/deg	71.800(3)	74.566(3)
Volume/Å^3	2333.08(13)	1786.44(12)
Z	2	2
D_{calc} /gcm^{-3}	1.698	1.700
μ(Mo-Kα)/mm^{-1}	10.854	5.392
F(000)	1196.0	924.0
Temperature/K	173(2)	173(2)
λ/Å	1.54178	1.54178
θ min, max/deg	3.674 / 68.225	4.052 / 68.242
Total, unique data	8489, 8246	6460, 6135
R1(obsd/all) [a]	0.0378 / 0.0387	0.0738 / 0.0761
wR2(obsd/all) [b]	0.1041 / 0.1051	0.1901 / 0.1915
Goodness-of-fit on F^2	1.075	1.150

[a] $R = \sum||F_O| - |F_C||/\sum|F_O|$. [b] $R_w = [\sum\omega(|F_O| - |F_C|)^2/\sum\omega F_O]^{1/2}$.

Table S3. Relative abundance of $^{16}O=^{16}O$, $^{16}O=^{18}O$, and $^{18}O=^{18}O$ generated during the oxidation of $H_2{}^{18}O$-labeled water by **1** and **3**.[a]

		relative abundance	
		observed [b]	theoretical [c]
1 O_2: 8.35 μmol TON = 2.4 (0.5 h)	$^{16}O=^{16}O$	0.0025±0.0010	0.0004
	$^{16}O=^{18}O$	0.0372±0.0021	0.0392
	$^{18}O=^{18}O$	0.9603±0.0031	0.9604
3 O_2: 8.28 μmol TON = 2.4 (3 h)	$^{16}O=^{16}O$	0.0036±0.0036	0.0004
	$^{16}O=^{18}O$	0.0348±0.0014	0.0392
	$^{18}O=^{18}O$	0.9616±0.0037	0.9604

[a] [Ru] = 3.5 mM, [Ce(IV)] = 70 mM, in 98% $H_2{}^{18}O$. [b] Relative ratios of dioxygen signals; standard deviations of no less than three trials are indicated in parentheses. [c] Probability of 98% $^{18}OH_2$-labeled water producing $^{36}O_2$, $^{34}O_2$, and $^{32}O_2$ is 0.9604, 0.0392, and 0.0004, respectively; values in table account for dilution factors; theoretical values assume both O-atoms of dioxygen are derived from water).

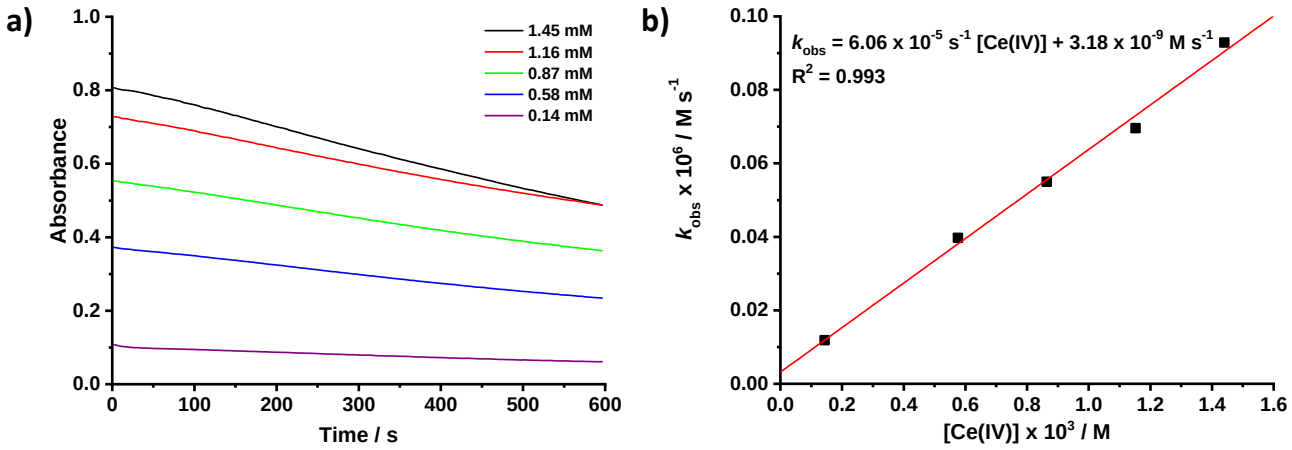

Fig. S1 a) Decay of Ce(IV) monitored at 360 nm after addition of **1** (10.3 μM) with various concentrations of Ce(IV) in 0.1 M HNO_3 at 20.0 °C; b) Plot of k_{obs} *vs* [Ce(IV)]. Zeroth-order rate constants were evaluated from the slope at 1 to 300 s.

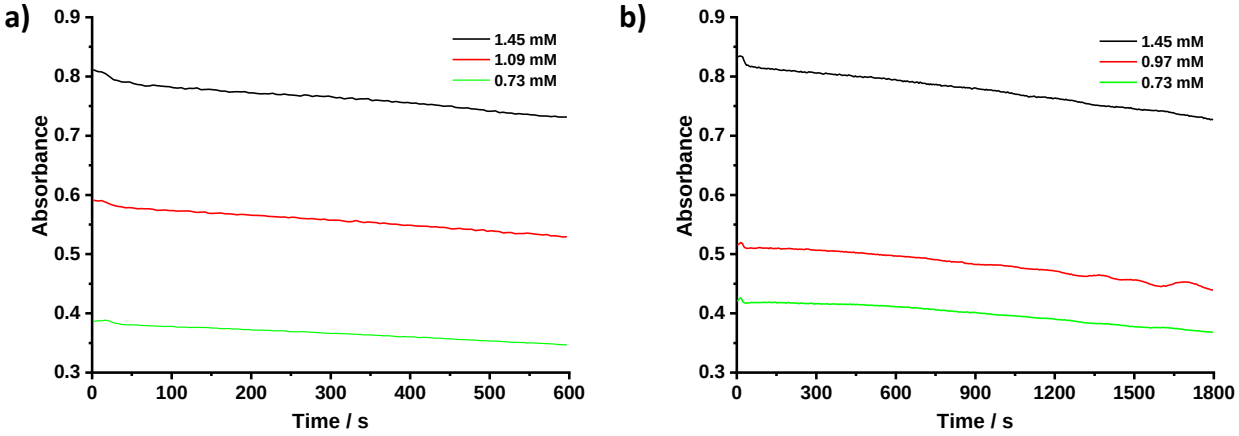

Fig. S2 Decay of Ce(IV) monitored at 360 nm after addition of a) **1** (1.0 μM) and b) **3** (1.0 μM) with various concentrations of Ce(IV) in 0.1 M HNO_3 at 20.0 °C

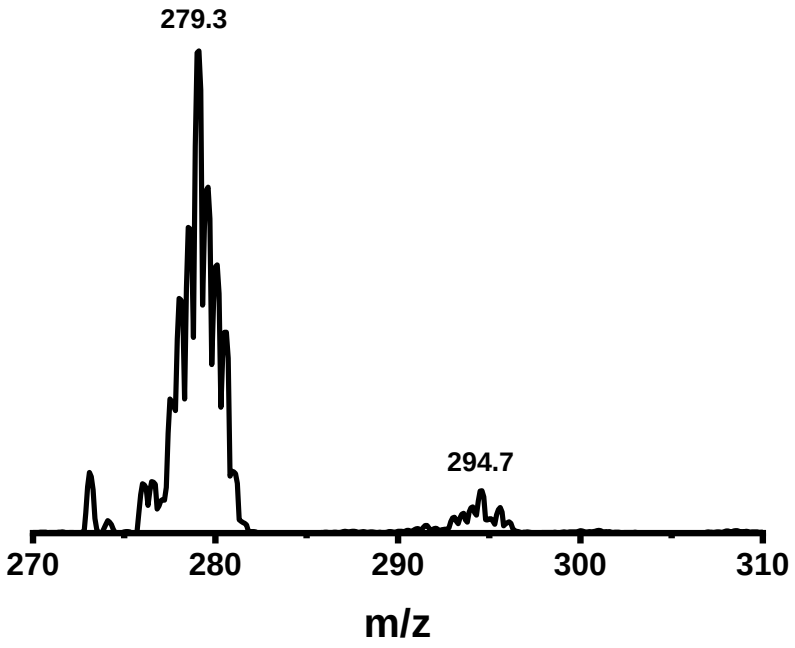

Fig. S3 ESI/MS of **1** (0.25 mM) in H_2O/CH_3CN (3:1 v:v) recorded immediately after the addition of 15 equiv. of Ce(IV).

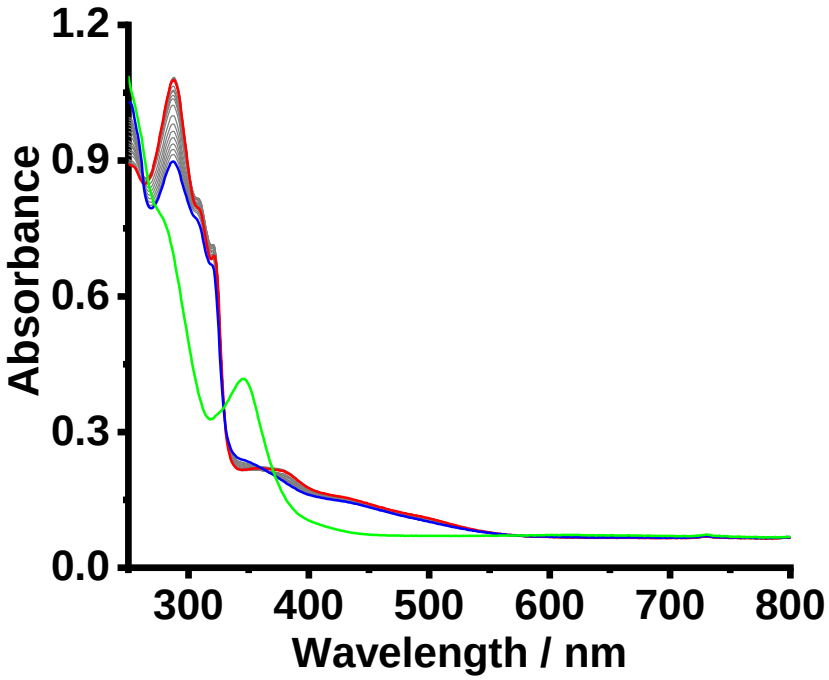

Fig. S4 UV/vis spectra changes of **1** (5.01×10^{-5} M) in 0.1 M HNO_3 (5% CH_3CN): recorded immediately after mixing with HNO_3 (red); recorded after 24 h (blue). UV/vis spectrum of **3** (green) (5.00×10^{-5} M) in 0.1 M HNO_3 (5% CH_3CN).

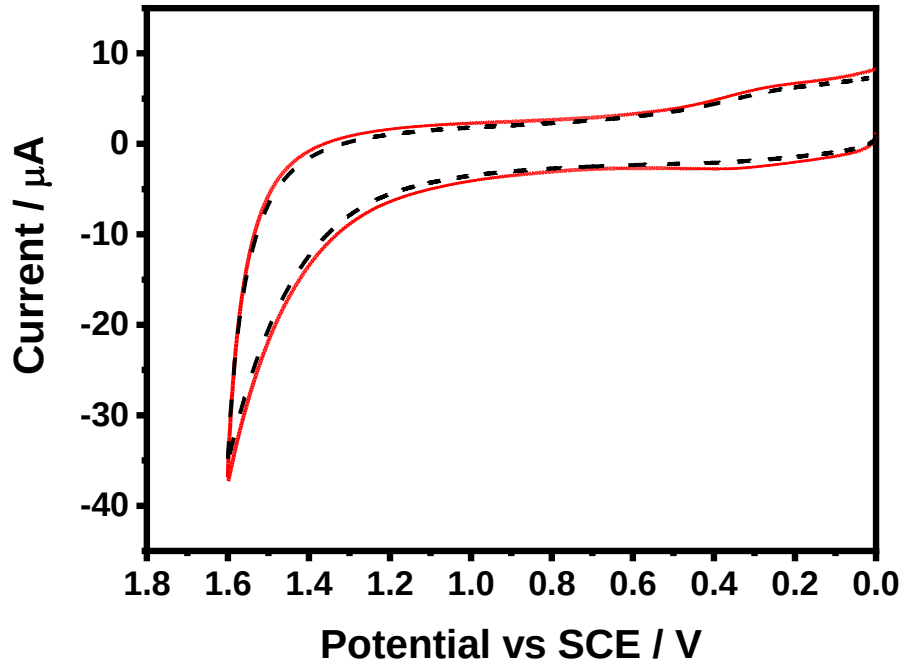

Fig. S5 CV of **3** (0.5 mM, solid) and blank (dash) in 0.1 M HNO_3/CH_3CN (3:1 v:v) at 20 ºC. Scan rate = 100 mV s^{-1}.

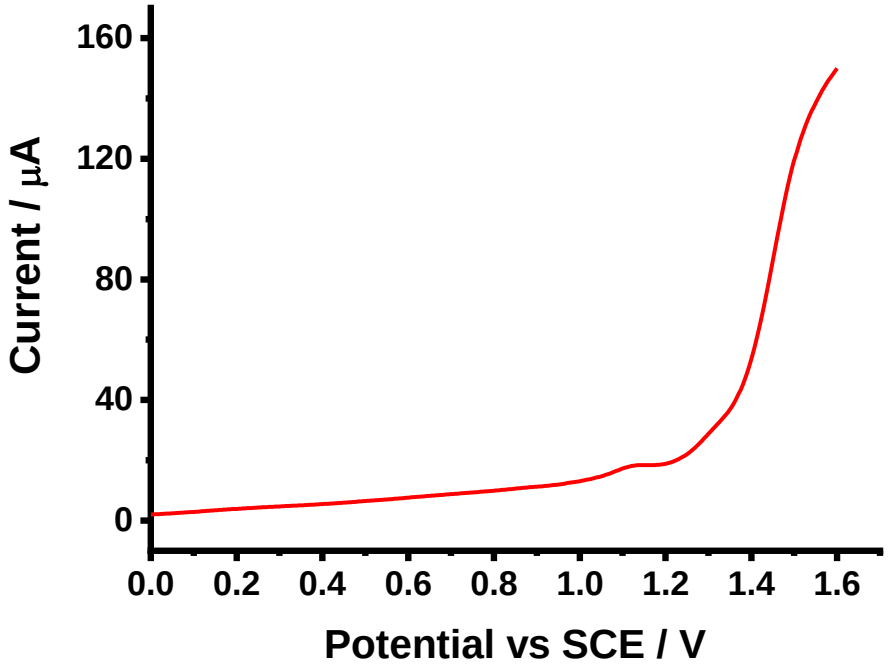

Fig. S6 Differential pulse voltammetry of **3** (0.2 mM) at pH 1 (0.1 M HNO_3) at r.t..

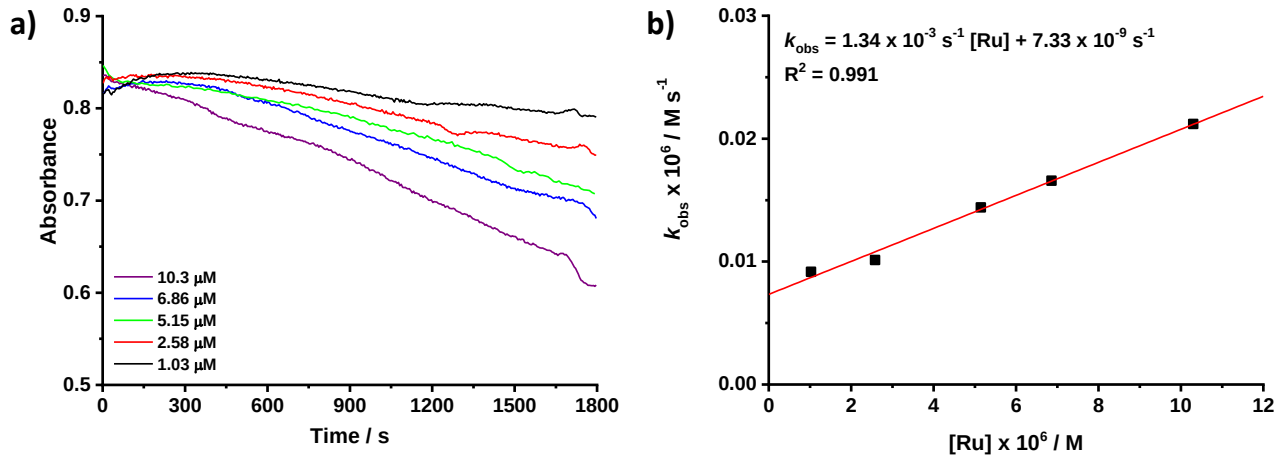

Fig. S7 a) Absorbance changes at 360 nm vs time for the reaction of various concentrations of **3** with Ce(IV) (1.44 mM) in 0.1 M HNO_3 at 20.0 °C; b) Plot of k_{obs} *vs* [**3**]. Zeroth-order rate constants were evaluated from 400 to 900 s, after the induction period.

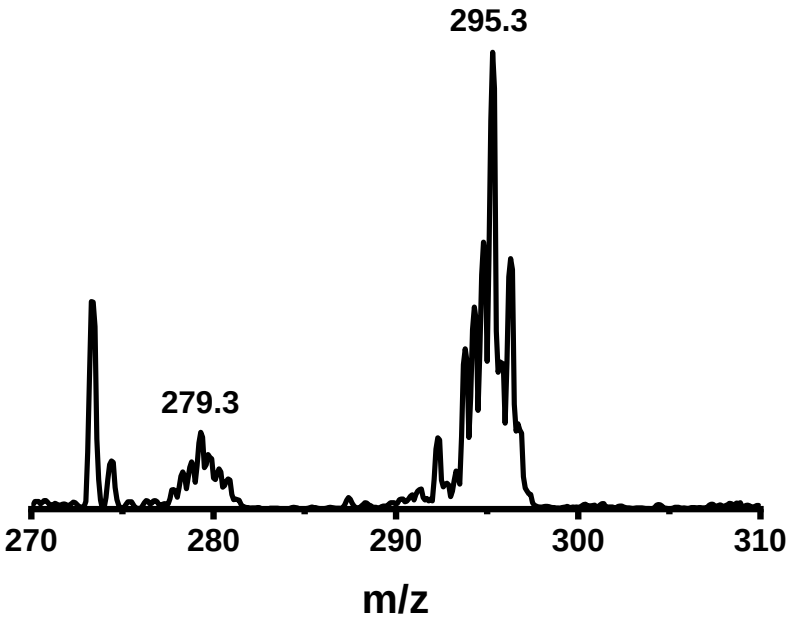

Fig. S8 ESI/MS of ^{15}N-**3** (0.50 mM) in H_2O/CH_3CN (4:1 v:v) recorded 60 min after the addition of 100 equiv. of Ce(IV). The solution was diluted 2 times by CH_3CN before injection. Notably, a small peak due to **1** (*m/z* = 279.3) (probably formed during the electrospraying process which is also observed in ESI/MS of neat ^{14}N-**3**) is recorded in MS before ^{15}N-**3** was treated with Ce(IV). After treatment with Ce(IV), the peak intensities ratios of **1** and **3** are unchanged.

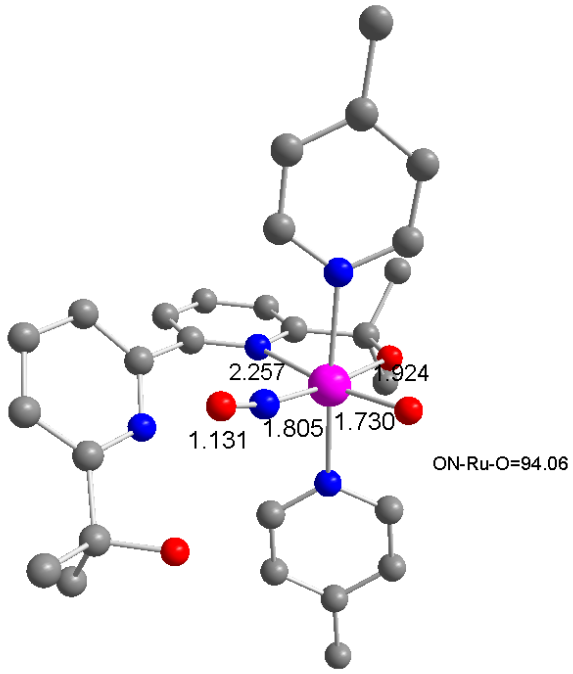

Fig. S9 Ball-and-stick representation of the optimized structures at the B3LYP level of theory for $[Ru(Hbdalk)(NO)(pic)_2(O)]^{2+}$. Color code: Ru, cyan; C, gray; N, blue; O, red; H atoms of the ligands were omitted for clarity.

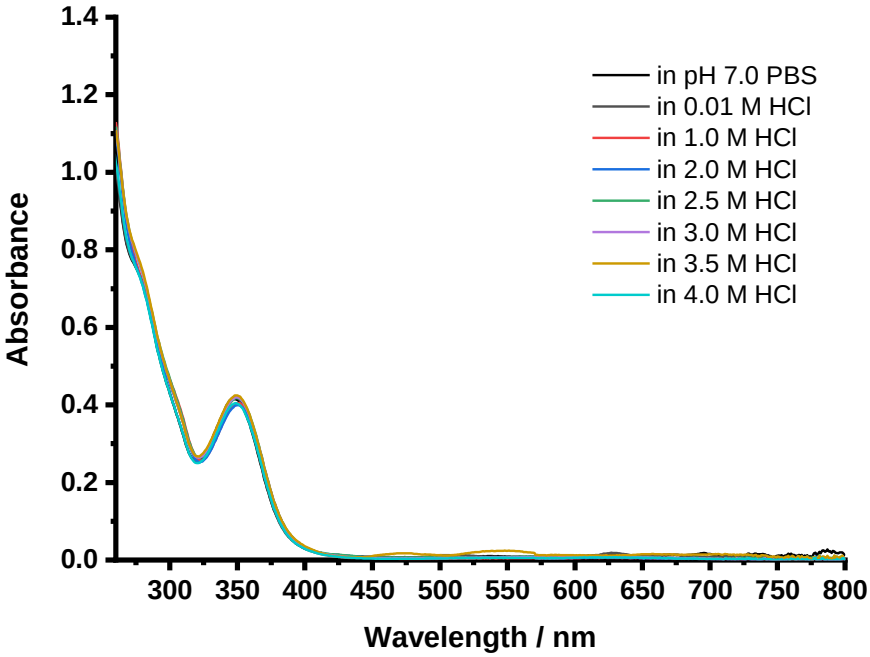

Fig. S10 UV/vis spectra of **3** (1.01×10^{-4} M) at pH 7.0 buffer and in the presence of various concentrations of HCl.

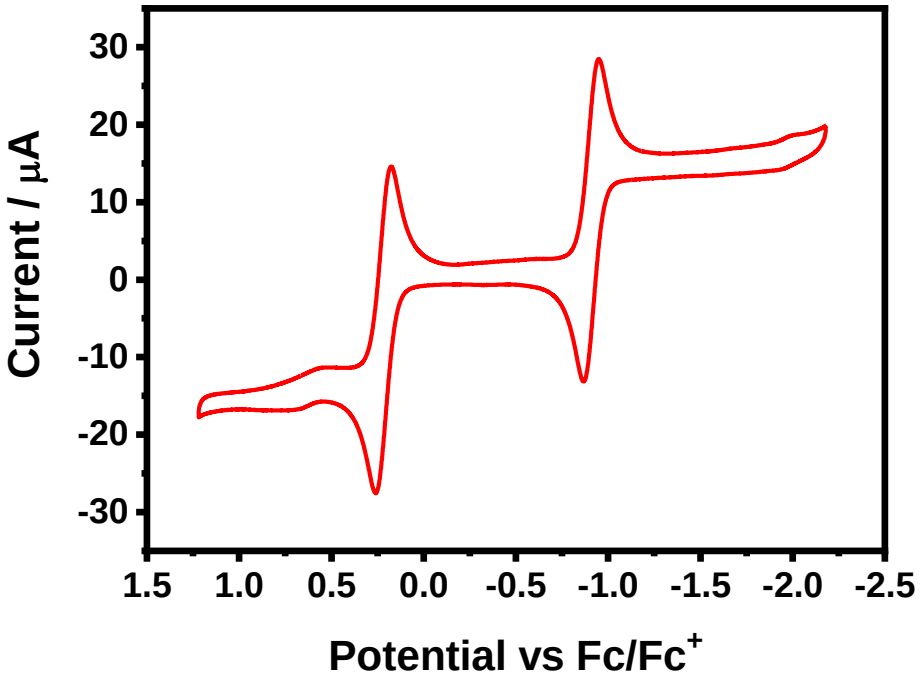

Fig. S11 CV of **1** (0.5 mM) in CH_3CN (0.1 M $^nBu_4PF_6$) at r.t.. Scan rate = 100 mV s^{-1}.

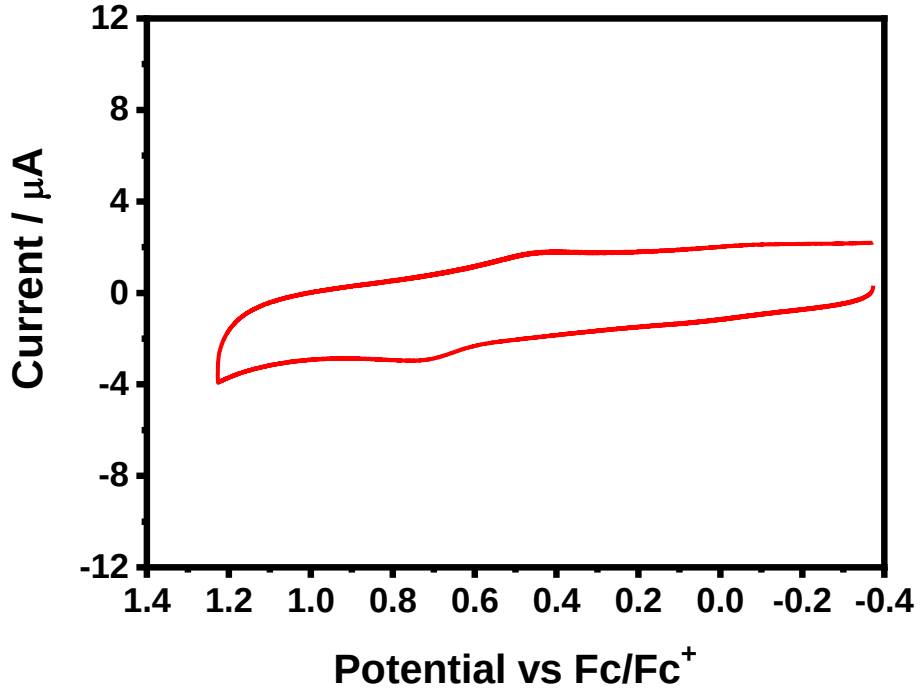

Fig. S12 CV of **3** (0.5 mM) in CH_3CN (0.1 M $^nBu_4PF_6$) at r.t.. Scan rate = 100 mV s^{-1}.

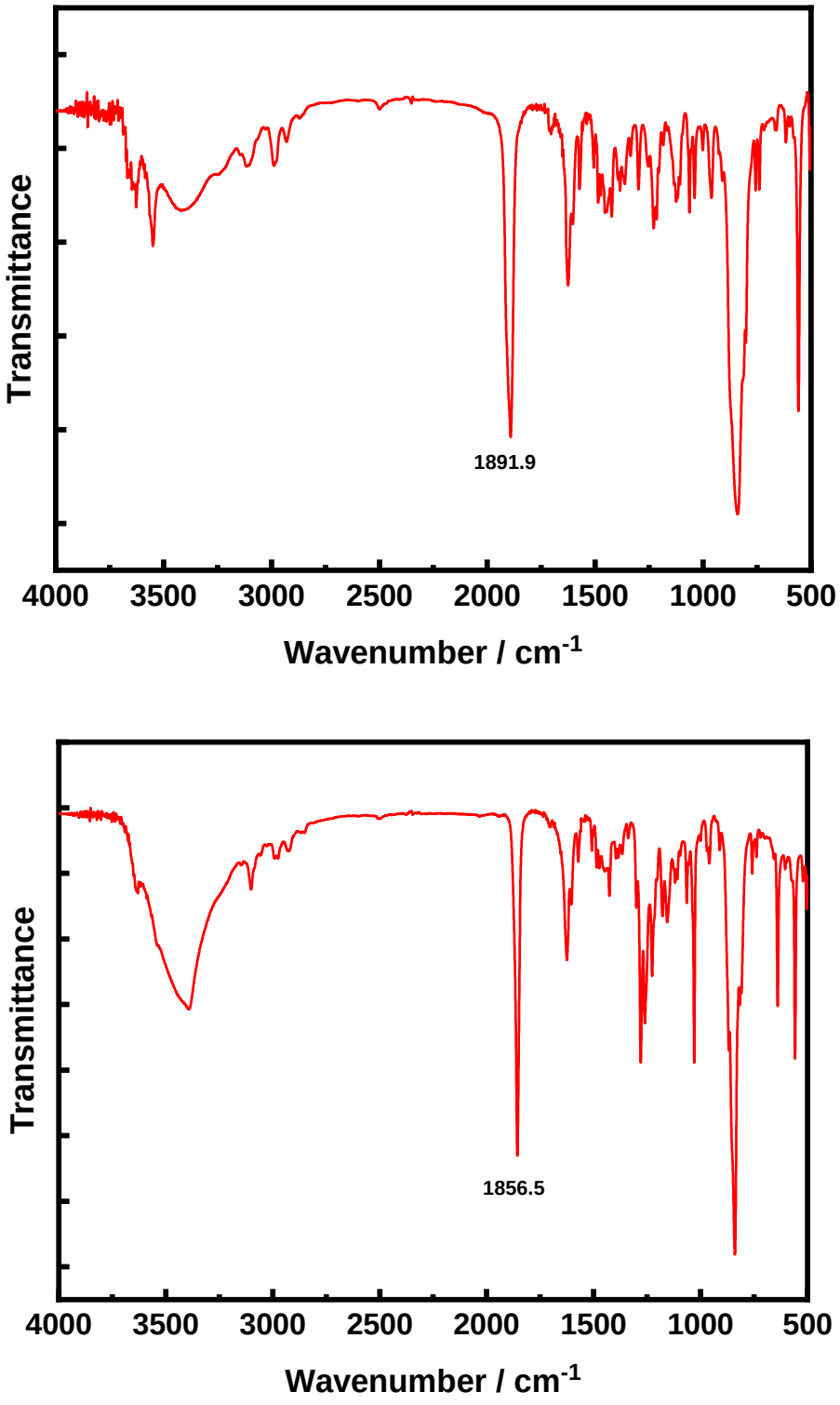

Fig. S13 IR spectra of ^{14}N-**3**[PF_6]$_2$ (top) and ^{15}N-**3**[PF_6]$_2$ (bottom).

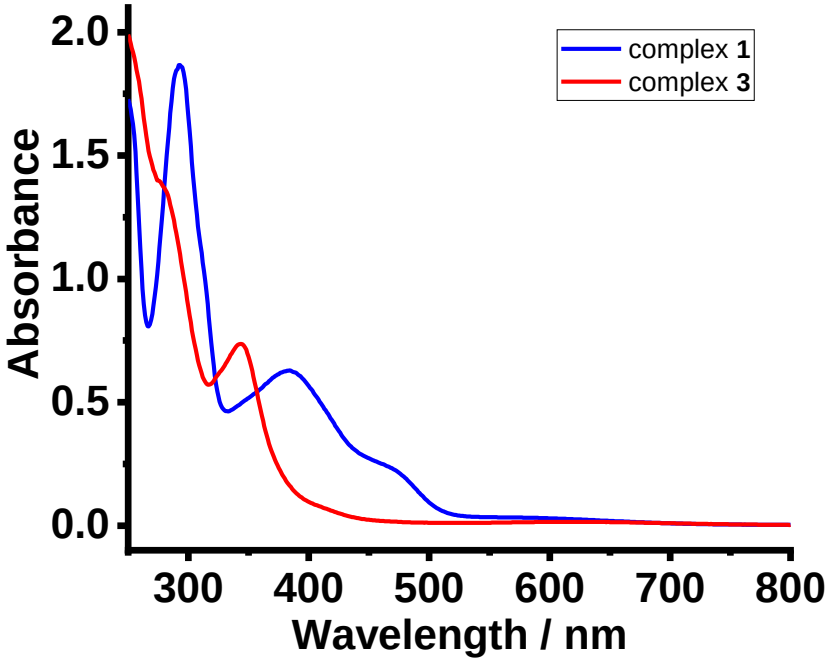

Fig. S14 UV/vis spectra of **1** (blue) and **3** (red) in CH_3CN (1.01×10^{-4} M).

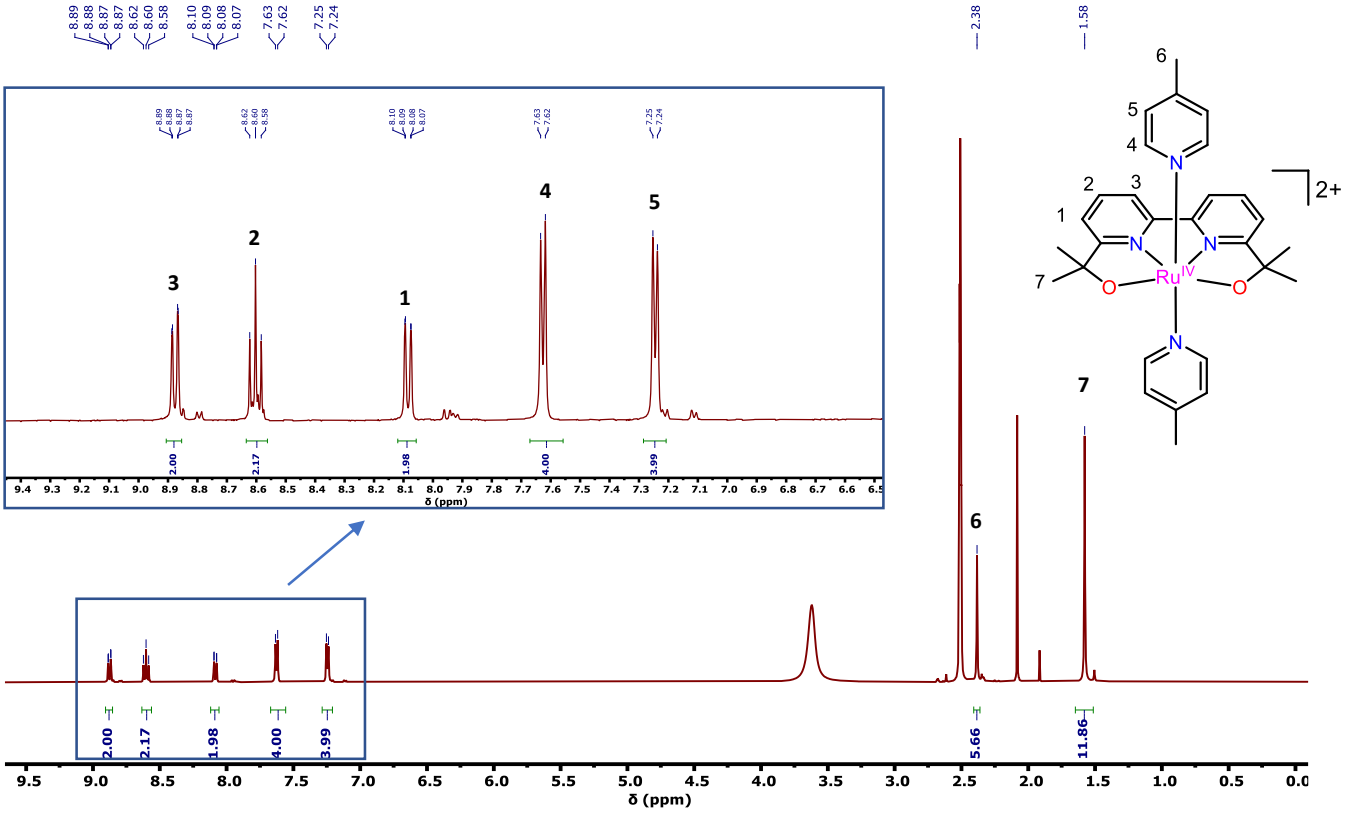

Fig. S15 ^{1}H NMR of **2**[$Ce(NO_3)_6$] in DMSO-d6.

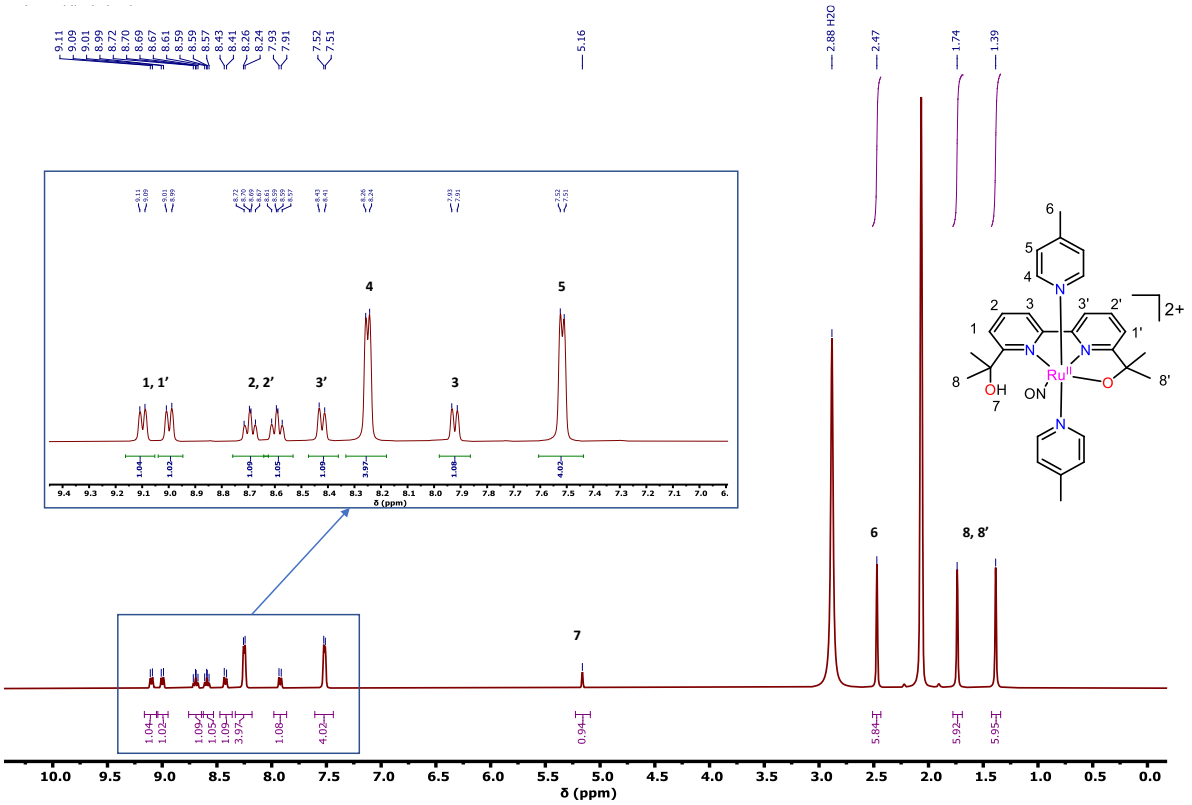

Fig. S16 ^{1}H NMR of **3**$[PF_6]_2$ in acetone-d6.

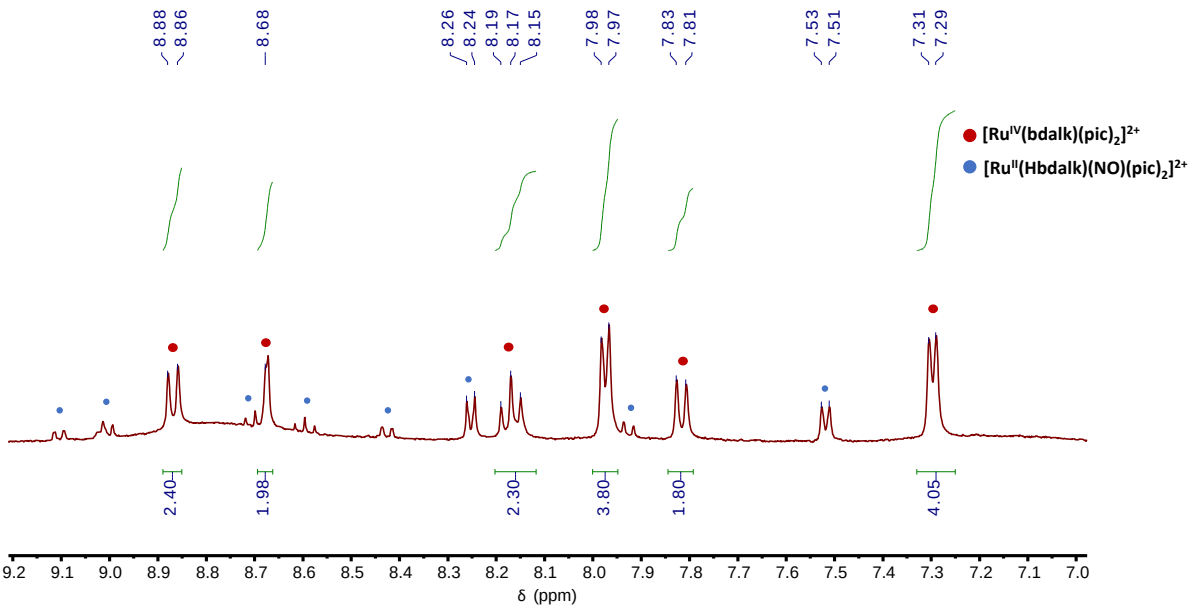

Fig. S17 ^{1}H NMR (in acetone-d6) of dark purple solid isolated from reaction of complex **1** + 1 equiv. of Ce(IV) in 0.01 M HNO_3/CH_3CN (2:1 v:v) followed by addition of excess NH_4PF_6 to the reaction solution. ESI/MS of obtained solid is consistent with $[Ru^{IV}(dalk)(pic)_2](PF_6)_2$ species, with minor Ru-NO impurities.

XYZ coordinates of $[Ru(Hbdalk)(NO)(pic)_2(O)]^{2+}$.

Ru	9.63976422458142	8.73604037616855	2.97013105128085
O	10.16113738722592	6.89068769185316	2.81188735025332
O	8.89964212279449	8.56819088505184	1.41547444511840
N	10.83625669641968	11.44202668779479	5.04934999318907
N	10.71179319898207	8.38898634374161	4.92583421320865
N	11.50029141857745	9.20514964455239	2.04935824195177
N	7.85260450359200	7.98507355135522	3.93268307326027
O	10.85132799311720	12.77466178799067	2.74834832458442
C	11.04247370361136	13.60137869826404	3.90688602477182
C	10.93153949447429	6.20667406555681	3.77796399792234
C	10.54901028241721	12.75175959489175	5.08894156508577
C	10.44935563437797	10.63530271548759	6.04309366977024
C	10.90613984010226	9.20796872126217	6.00865481099418
C	11.18350850895989	7.11289267844403	4.97393958396784
C	12.37220056381603	10.10304239984023	2.55112978663395
C	11.80453962530719	8.53987492324455	0.90738123592834
C	7.31176192740479	8.52935858091842	5.04297741944477
C	7.22357830072336	6.94434993170118	3.34007437530908
C	9.85525004895948	13.30503968102128	6.17794893461306
C	9.43651324496467	12.47064414177780	7.21474990270148
C	9.73234370368357	11.10783156782780	7.15525262572986
C	11.57600299885745	8.74561349064903	7.14403414127455
C	12.07237444414957	7.44164398574952	7.18884905234775
C	11.87442129299028	6.62157524846004	6.08795915347160
C	12.53984367935852	13.90679521680641	4.09861485990618
C	10.24055046791741	14.89797944407323	3.73564182912382
C	12.27320272292440	5.79264843301369	3.12677305802948
C	10.14233083524627	4.94706036868759	4.20133126974320
C	13.59079477161220	10.35084265718636	1.92500218266741
C	13.93800630679229	9.68466631339493	0.74039781240961
C	12.99491734231292	8.76318361665952	0.23683682114768
C	15.23016774022156	9.94168250366432	0.02535503016108
C	6.12748063729340	8.05661766565979	5.59354718676597
C	5.44463819745682	6.98382547779052	4.99312069997115
C	6.03387821112547	6.43340773658721	3.83785836261312
C	4.15553841481899	6.45045832224473	5.54039840835021
N	9.01593368170161	10.41039817824859	3.22858950804229
H	11.09235423413371	13.29919674399824	1.97115646441100
H	11.06904987370280	7.82106058917437	0.54411662267580
H	7.84251897980004	9.36426249679124	5.50509635581508
H	7.69827680681991	6.52714873659821	2.45060672745081
H	9.63615761684456	14.37173055770391	6.21752599367013

H	8.88299197227077	12.88038145606404	8.06331205012683
H	9.41696968785494	10.43116419202640	7.95218442770578
H	11.73512597075218	9.42667433411476	7.98073673668038
H	12.60959673827849	7.07993749946813	8.06911042799671
H	12.24524948655736	5.59635750043010	6.08433511742664
H	12.92470124547156	14.46718821451690	3.23080743678947
H	13.11713874981229	12.97588738144747	4.20063309418443
H	12.71402979546227	14.52068990716668	4.99547994332415
H	10.57420310660842	15.41465345319844	2.82124238862217
H	10.39624635546142	15.60189578464996	4.56621611905450
H	9.16396481480806	14.69306870530386	3.63702687216416
H	12.05787813615120	5.21295102645288	2.21753477859679
H	12.86766499906788	5.16163050829803	3.80365837329122
H	12.87354587125628	6.67173758180350	2.85319397059503
H	9.90377858896422	4.36500451555095	3.29935790695090
H	9.20352110560499	5.21637486638713	4.70678181942152
H	10.72973235032417	4.30649476581065	4.87500482227286
H	14.26841010094714	11.08073750190000	2.37296504662458
H	13.18593341238088	8.21621076540902	-0.68954160172705
H	15.73355404162053	8.99594451454834	-0.23165203013701
H	15.91684052323829	10.55773632834454	0.62167480193918
H	15.03824843429670	10.46606246777906	-0.92710421203844
H	5.73456587289877	8.53484380559368	6.49328814230926
H	5.55913714472858	5.60257248925138	3.31025388279218
H	4.25465243491482	5.38051312690874	5.78916761344505
H	3.35667709897012	6.52553780571429	4.78362284260683
H	3.83322420071728	6.98957386973059	6.44121086864533
H	12.06574396934941	10.63146835290266	3.45835060841274
O	8.45994211105844	11.36673482734027	3.46330558615653